CrossMark

Effects of MoS₂ and Multiwalled Carbon Nanotubes on Tribological Behavior of TiAl Matrix Composite

Kang Yang, Xiaoliang Shi, and Wenzheng Zhai

The sliding velocities and applied loads are often varied to minimize friction and decrease mechanical energy dissipation in moving mechanical assemblies. In this study, TiAl matrix composites containing MoS₂ and multiwalled carbon nanotubes (MWCNTs) are fabricated using spark plasma sintering. The testing conditions are chosen as 0.3 m/s-6.5 N; 0.5 m/s-11.4 N; and 0.7 m/s-16.3 N. The sliding tribological property of TiAl matrix composite containing MoS₂ and MWCNTs (TMC-MM) is evaluated based on a ball-on-disk tribometer. The results show that the tribological performance of TMC-MM is excellent for the lower friction coefficient and less wear rate at 0.7 m/s-16.3 N. Massive MWCNTs are pulled out from TMC-MM at 0.7 m/s-16.3 N, and made to adhere to wear surface due to the existence of MoS₂ with high adhesion property, resulting in the formation of smooth isolated island-like layer. It could protect the lubrication film formed on the worn surface, and be beneficial to the excellent tribological behavior of TMC-MM.

1. Introduction

In recent years, TiAl alloys have attracted the increased attention of many researchers in view of their eminent mechanical characteristics and thermal behavior (Ref 1-4). The failure of 80% mechanical components has been caused because of the poor tribological behavior of materials including TiAl alloys. Hence, it is necessary to improve the tribological property of TiAl alloys by fabricating TiAl matrix self-lubricating composite.

Many tribological researchers, e.g., Cheng et al. (Ref 5) and Sun et al. (Ref 6) fabricated TiAl matrix self-lubricating composite by adding solid lubricants, and investigated the tribological behavior using the method of friction tests. Cheng et al. (Ref 5) investigated the tribological behavior of TiAl intermetallics containing TiB₂. The results showed that the tribological behavior of TiAl alloys was significantly enhanced with the addition of solid lubricant TiB₂. Sun et al. (Ref 6) studied the tribological behavior of Ti₂AlN/TiAl composite and found that the friction coefficients were continually lowered, while the wear rates were continuously enhanced with the increasing applied load. Shi et al. (Ref 7) fabricated TiAl matrix self-lubricating composite containing 10 wt.%Ag (TiAl-10 wt.%Ag) and found that the tribological behavior of TiAl-10 wt.%Ag was excellent at 25-800 °C, compared to that of TiAl-based alloy. Li et al. (Ref 8) employed solid lubricant MoS₂ with lamellar structure to fabricate Nickel matrix self-lubricating composite, and found that friction coefficient slightly increased during the layer separation of MoS₂.

Mahathanabodee et al. (Ref 9) fabricated SS316L matrix composite by adding the solid lubrications of h-BN and MoS₂. It was found that the friction coefficient of SS316L matrix composite was lowered by solid lubricant h-BN, while the wear resistance was significantly improved by MoS₂ with high adhesion behavior. Ahmad et al. (Ref 10) studied the wear resistance of Al₂O₃ nanocomposites containing multiwalled carbon nanotubes (MWCNTs). The results showed that the wear resistance of monolithic Al₂O₃ was significantly improved by MWCNTs with tubular structure. Bastwros et al. (Ref 11) studied the tribological behavior of Aluminum-carbon nanotube matrix composite (Al-CNTs), and found that the wear resistance of Al-CNTs significantly increased. To the best of our knowledge, few works have reported the synergetic enhancement effects of MoS₂ and MWCNTs on the tribological performance of a TiAl matrix composite at 0.3 m/s-6.5 N, 0.5 m/s-11.4 N, and 0.7 m/s-16.3 N.

The sliding velocities and applied loads are often varied to minimize friction and decrease mechanical energy dissipation in moving mechanical assemblies. In this study, TiAl matrix composite containing MWCNTs and MoS₂ (TMC-MM) is chosen to act as the testing material of sliding wear. The sliding friction and wear tests of 80-min sliding are continuously carried out on the ball-on-disk tribometer of HT-1000 at 0.3 m/s-6.5 N, 0.5 m/s-11.4 N, and 0.7 m/s-16.3 N, respectively. The sliding friction and wear behaviors of TMC-MM at 0.3 m/s-6.5 N and at 0.7 m/s-16.3 N are analyzed using the electron probe microanalysis of JAX-8230 and the field emission scanning electron microscope (FESEM) of SIRION 200.

2. Experimental Details

2.1 Materials

TiAl matrix composite (48 at.%Ti-47 at.%Al-2 at.%Cr-2 at.%Nb-1 at.%B) containing 5 wt.%MoS₂ and 1 wt.%MWCNT is fabricated by spark plasma sintering (SPS). The commercially available powders (less than 25 μm in average size, more than 95% in purity) are chosen for this study. Before SPS process, the

Kang Yang, Xiaoliang Shi, and **Wenzheng Zhai**, School of Mechanical and Electronic Engineering, Wuhan University of Technology, 122 Luoshi Road, Wuhan 430070, China. Contact e-mail: sxl071932@126.com.

raw powders are mixed in the teflon vials using the vibration milling (45Hz in vibration frequency). After being mixed and then dried, the dried powder is sintered for 5 min using the apparatus of D.R. Sinter® SPS3.20 (Sumitomo Coal & Mining, now SPS Syntex Inc. Japan) at the temperature of 1200 °C and at the pressure of 30MPa under the protection of pure Ar atmosphere.

2.2 Vicker's Microhardness and Density

Using the instrument of HVS-1000 (Changzhou detu Precision Instrument Co Ltd., China), the mean Vicker's hardness (5.3 GPa) of TMC-MM is obtained by carrying out ten tests according to the ASTM standard E92-82 (Ref 12). Archimedes' principle is strictly executed to attain the mean density (3.6 g/cm^3) of TMC-MM according to the ASTM Standard B962-08 (Ref 13).

2.3 Tribological Test

The friction tests of 80-min sliding are carried out on the ball-on-disk tribometer of HT-1000 (Zhong Ke Kai Hua Corporation, China) according to the ASTM Standard G99-95 (Ref 14). The disks of TMC-MM are cleaned with acetone and then dried in hot air before testing. The TMC-MM disks rotate against the GCr15 balls of 6 mm in diameter at room temperature and at the relative humidity of 65-70%.

2.4 Microstructural Analysis

The surfaces of TMC-MM are examined by XRD with CuKα radiation at 30 kV and 40 mA at a scanning speed of 0.01 s^{-1}. The morphologies of wear scars of TMC-MM are characterized by the electron probe microanalysis (EPMA) of JAX-8230 (JEOL Corporation, Japan). The cross-sectional morphologies of wear scars of TMC-MM are analyzed by the field emission scanning electron microscope (FE-SEM) of SIRION 200 (JEOL Corporation, Japan).

3. Results and Discussion

3.1 Molecular Structure of MWCNTs and MoS$_2$

Figure 1 shows the typical molecular structures and FESEM micrographs of MWCNTs. As described in the paper of Fang et al. (Ref 15), the multilayer and tubular molecular structure of MWCNTs could be clearly seen in Fig. 1(a). The FESEM micrograph of MWCNT powder is exhibited in Fig. 1(b).
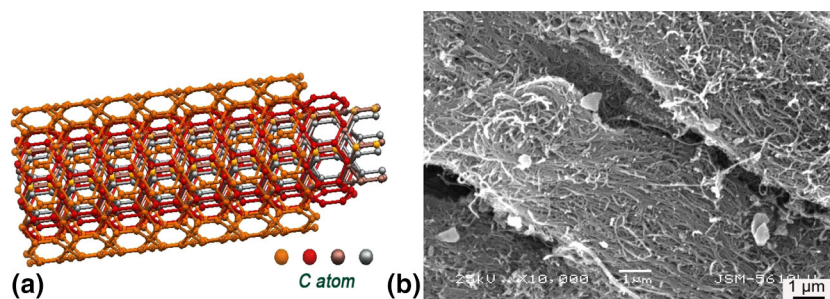
Figure 2 shows the typical FESEM micrograph of MWCNTs in the fractured surface of TMC-MM. As shown in Fig. 2, MWCNTs (about 40-50 nm in diameter) are tightly combined with TiAl-based alloy matrix.

Figure 3 shows the representative molecular structure and FESEM micrograph of MoS$_2$. According to the report of Ma et al. (Ref 16), the typical multilayer molecular structure of MoS$_2$ can be better understood, as shown in Fig. 3(a). Figure 3(b) shows the FESEM micrograph of MoS$_2$ powder.

3.2 Compositions of TMC-MM

Figure 4 shows the typical XRD pattern of TMC-MM prepared by SPS. As shown in Fig. 4, TMC-MM is mainly composed of TiAl, MWCNTs, and MoS$_2$.

3.3 Friction Coefficient and Wear Rate

During the 80-min sliding wear, the friction coefficient of TMC-MM is automatically recorded by the control system of HT-1000 with the increasing real time. The wear rate W of TMC-MM is defined as Formula 1 (Ref 17):

$$W = \frac{V}{F \cdot L} = \frac{2\pi \cdot r \cdot A}{F \cdot L} \qquad \text{(Eq 1)}$$

where V is the wear volume, F is the applied load, and L is the sliding distance, and r is the friction radius. A, which is the cross-sectional area of wear scar, can be obtained using
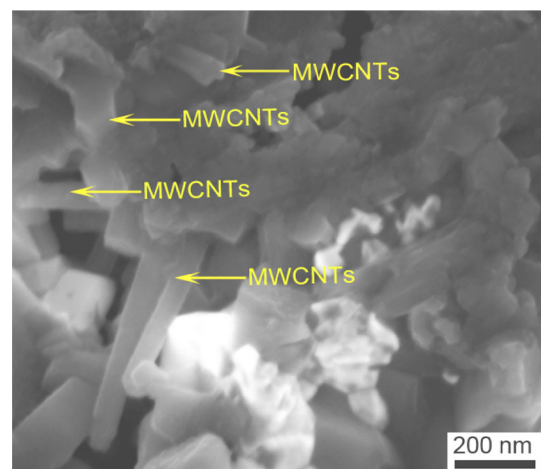

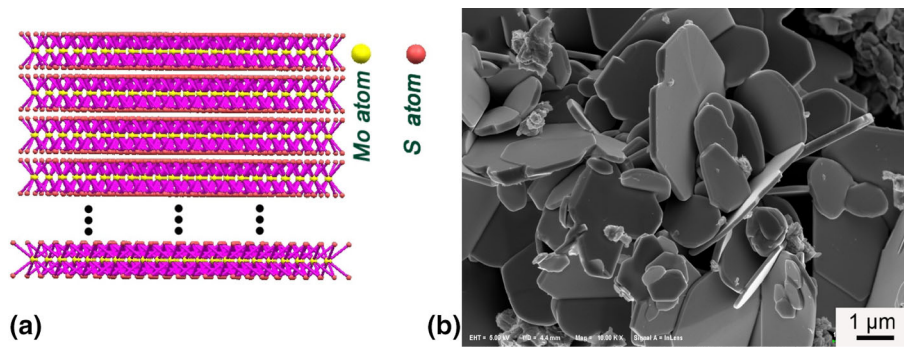**Fig. 2** Typical FESEM micrograph of MWCNTs in the fractured surface of TMC-MM

Fig. 1 Typical molecular structure and FESEM micrograph of MWCNTs: Molecular structure (a) and FESEM micrograph (b)

Fig. 3 Representative molecular structure and FESEM micrograph of MoS$_2$: Molecular structure (a), and FESEM micrograph (b)
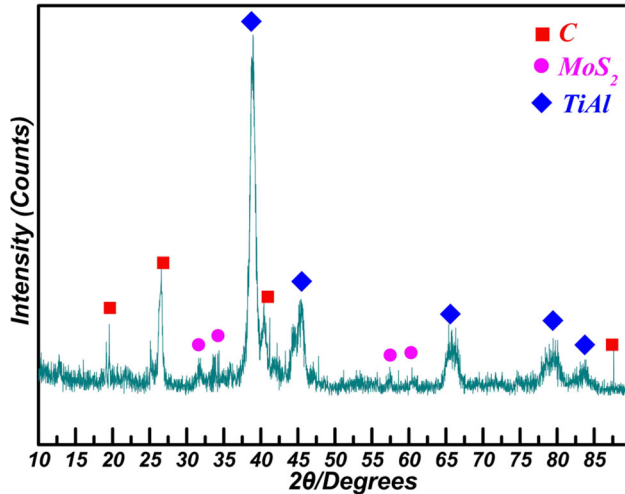

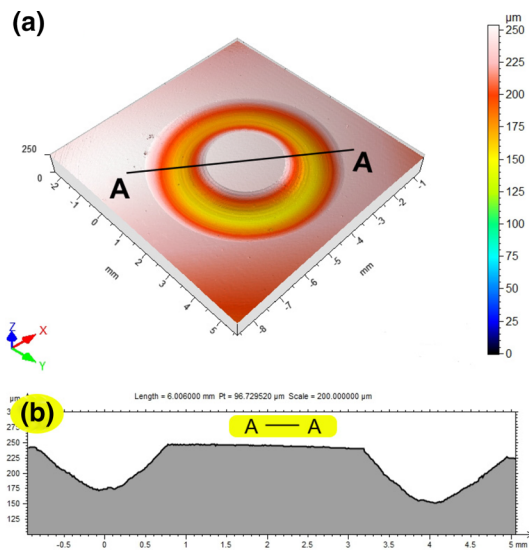**Fig. 4** Typical XRD pattern of TMC-MM prepared by SPS

Fig. 5 Typical morphology of wear scar of TMC-MM sliding against GCr15 ball: 3D profile of wear scar (a) and 2D profile of wear scar (b)

the surface profiler of ST400 (Nanovea Corporation, America). As shown in Fig. 5, when the profilometer stylus slowly moves across wear scar along the straight line of AA (see Fig. 5a), the coordinate positions of stylus are continuously recorded to form a 2D profile (see Fig. 5b). The three friction tests are repeatedly executed to obtain the mean cross-sectional areas, A, of wear scars at 0.3 m/s-6.5 N, 0.5 m/s-11.4 N, and 0.7 m/s-16.3 N, respectively.

Figure 6 shows the typical friction coefficients of TiAl-based alloy at 0.3 m/s-6.5 N; and TMC-MM at 0.3 m/s-6.5 N, 0.5 m/s-11.4 N, and 0.7 m/s-16.3 N, respectively. As shown in Fig. 6, the friction coefficients of TMC-MM are significantly lower than those of TiAl-based alloy. The friction coefficients of TMC-MM are poor at 0.3 m/s-6.5 N (see curves A and B), compared to those at 0.5 m/s-11.4 N (see curves C and D). The friction coefficients of TMC-MM are excellent at 0.7 m/s-16.3 N (see curves E and F).

Figure 7 shows the mean wear rates of TiAl-based alloy at 0.3 m/s-6.5 N; and TMC-MM at 0.3 m/s-6.5 N, 0.5 m/s-11.4 N, and 0.7 m/s-16.3 N, respectively. As shown in Fig. 7, the high mean wear rate of TiAl-based alloy is obtained, compared to that of TMC-MM at 0.3 m/s-6.5 N. The mean wear rate 2.7×10^{-4} mm^3/N m of TMC-MM at 0.3 m/s-6.5 N is higher than 2.0×10^{-4} mm^3/N m at 0.5 m/s-11.4 N. TMC-MM obtains the lower mean wear rate of 1.5×10^{-4} mm^3/N m at 0.7 m/s-16.3 N.

With reference to Fig. 6 and 7, the tribological behaviors of TMC-MM are excellent at 0.7 m/s-16.3 N and poor at 0.3 m/s-6.5 N.

The wear resistance of TMC-MM is in close relation with its mechanical property. Material hardness is regarded as the particularly important parameter of mechanical property. Consequently, the effect of subsurface hardness of wear scar (SHWS) on the tribological behavior of TMC-MM would be further studied at 0.3 m/s-6.5 N and 0.7 m/s-16.3 N, respectively.

3.4 Influence of SHWS on Tribological Behavior of TMC-MM

Figure 8 shows the measured locations of subsurface hardness of wear scar (SHWS) marked by twelve red spheres. As shown in Fig. 8, the angle between the first measured location and X axis is chosen as 30°. Figure 9 shows the SHWS of twelve measured locations at 0.3 m/s-6.5 N and 0.7 m/s-16.3 N. As shown in Fig. 9, the higher SHWS 8.2GPa is acquired at 0.7 m/s-16.3 N, compared to SHWS 7.0 GPa obtained at 0.3 m/s-6.5 N.
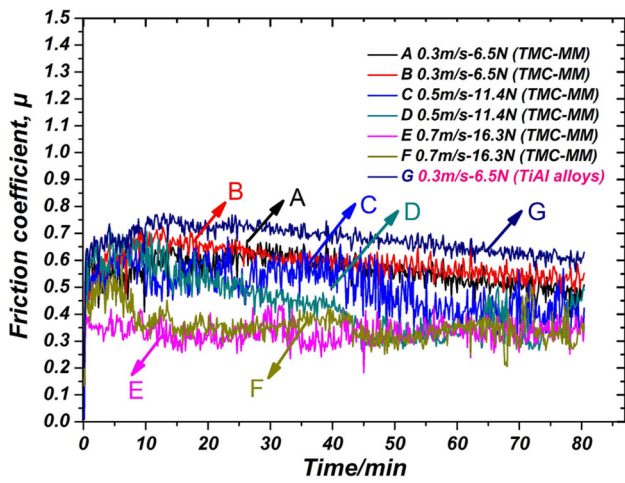
Fig. 6 Typical friction coefficients of TiAl-based alloy at 0.3 m/s-6.5 N; and TMC-MM at 0.3 m/s-6.5 N, 0.5 m/s-11.4 N, and 0.7 m/s-16.3 N
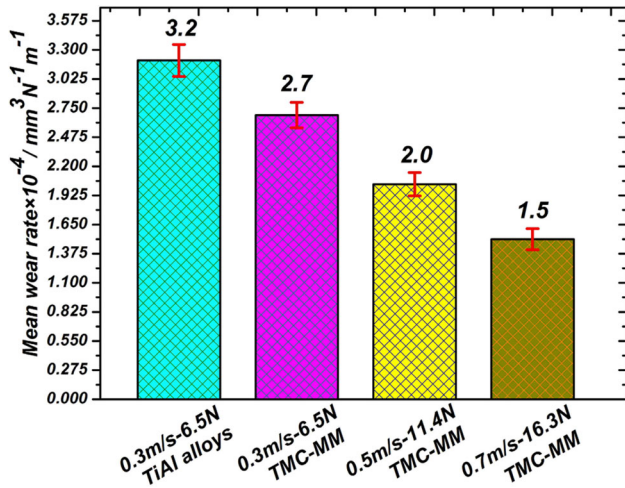

Fig. 9 SHWS values of twelve measured locations at 0.3 m/s-6.5 N (G) and 0.7 m/s-16.3 N (H)

Fig. 7 Mean wear rates of TiAl-based alloy at 0.3 m/s-6.5 N; and TMC-MM at 0.3 m/s-6.5 N, 0.5 m/s-11.4 N, and 0.7 m/s-16.3 N
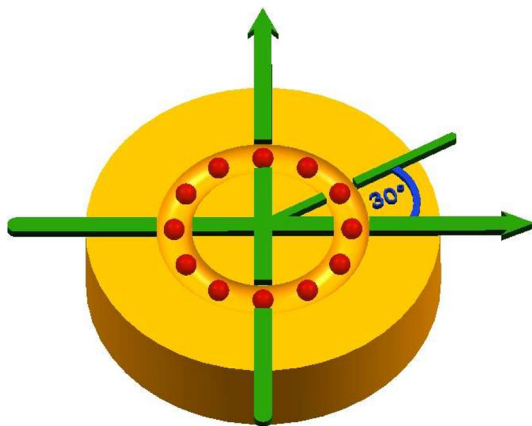

Fig. 8 Measured locations of subsurface hardness of wear scar (SHWS) marked by twelve red spheres (Color figure online)
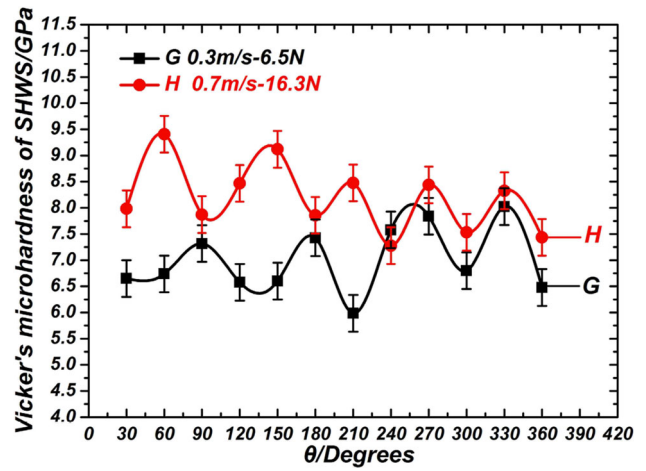
The wear resistance of material is in close relation with its mechanical behavior. Hence, the wear volume V of TMC-MM can be defined as Formula 2 (Ref 18).

$$V = a \cdot \frac{F^{9/8}}{K_{IC}^{1/2} \cdot H^{5/8}} \cdot \left(\frac{E}{H}\right)^{4/5} L \qquad \text{(Eq 2)}$$

where V is the wear volume, F is the applied load, K_{IC} is the fracture toughness, H is the SHWS, L is the sliding distance, and a is known as real constant.

The wear rate W of TMC-MM is additionally expressed as Formula 3 by substituting Formula 2 into Formula 1:

$$W = \frac{V}{F \cdot L} = a \cdot \frac{F^{1/8}}{K_{IC}^{1/2} \cdot H^{5/8}} \cdot \left(\frac{E}{H}\right)^{4/5} \qquad \text{(Eq 3)}$$

As shown in Formula 3, it is found that the wear rate W of TMC-MM is inversely proportional to its SHWS. Hence, the small mean wear rate (1.5×10^{-4} mm^3/N m) at 0.7 m/s-16.3 N is obtained for the high SHWS of 8.2GPa. The high mean wear rate of TMC-MM (2.7×10^{-4} mm^3/N m) is acquired at 0.3 m/s-6.5 N for the small SHWS of 7.0 GPa.

In order to better explore the synergetic enhancement effect of MoS$_2$ and MWCNTs on the tribological behavior of TMC-MM, the content and distribution of MoS$_2$ and MWCNTs need to be evaluated by observing wear scar morphologies obtained after tests at 0.3 m/s-6.5 N and 0.7 m/s-16.3 N, respectively.

3.5 Wear Mechanism And Structural Features

Figure 10 exhibits the typical wear scar morphologies, backscattered image, and the FESEM morphologies of MWCNTs after 80-min sliding. Massive shallow peeling pits and isolated island-like (patchy) layers appear on wear scar (see Fig. 10a). It is obvious that the dominant wear mechanisms at 0.3 m/s-6.5 N are plouw and peeling. As shown in Fig. 10(b), a few deep peeling pits and isolated island-like (patchy) layers appear on wear scar. It is evident that the primary wear mechanism is peeling at 0.7 m/s-16.3 N. As can be seen in Fig. 10(c), MWCNTs are uniformly exposed to wear scar, and covered by MoS$_2$ at 0.3 m/s-6.5 N (see the regions marked by
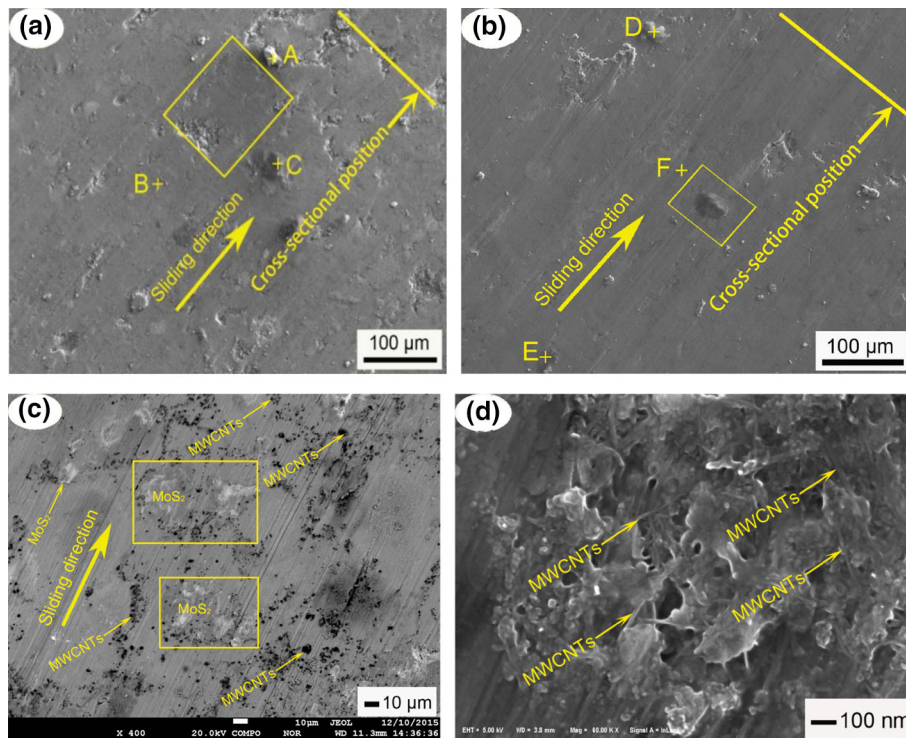
Fig. 10 Typical wear scar morphologies, backscattered image, and FESEM morphologies of MWCNTs after 80-min sliding: wear scar morphology at 0.3 m/s-6.5 N (a), wear scar morphology at 0.7 m/s-16.3 N (b), backscattered image at 0.3 m/s-6.5 N (c), and FESEM morphologies of MWCNTs at 0.7 m/s-16.3 N (d)

Table 1 Elemental compositions (at.%) of measured regions marked by A, B, and C in Fig. 10(a)

Element	C	Mo	S	O	Fe	Ti	Al	Cr	Nb	Si
A	-	1.27	1.34	28.75	3.06	28.57	34.37	1	0.84	0.79
B	3.76	1.55	1.71	5.69	0.32	36.02	49.85	1.1	…	…
C	…	1.4	1.45	13.3	0.56	31.83	49.16	1.23	0.08	0.98

rectangles in Fig. 10c). As shown in Fig. 10(d), massive MWCNTs pulled out from TMC-MM are tightly adhered by MoS_2 on to the wear surface and accumulated into the isolated island-like (patchy) layers at 0.7 m/s-16.3 N.

Table 1 shows the elemental compositions of measured regions marked by A, B, and C (see Fig. 10a). As shown in Table 1, the regions marked by A and C contain abundant quantity of oxygen (O) element. It indicates that massive oxides are formed at 0.3 m/s-6.5 N during the dry sliding wear. As shown in the measured region marked by B, massive elements of C, Mo, and S appear on the smooth wear scar, compared to those in the measured regions marked by C and A.

Figure 11 shows the microstructural and elemental distributions of local wear scar marked by rectangle in Fig. 10(a). As shown in Table 1 and Fig.11, the appearances of C, Mo, and S elements further demonstrate that MWCNTs are uniformly exposed to wear scar because of the effect of sliding frictional force, and covered by MoS_2 with lubricating property, resulting in the smaller SHWS (7.0GPa).

Table 2 exhibits the elemental compositions of measured regions marked by D, E, and F (see Fig. 10b). As shown in the region marked by D in Table 2, the wear debris obtained at 0.7 m/s-16.3 N are mainly composed of alumina, iron oxide,

and molybdic oxide. In the region marked by E, the smooth isolated island-like (patchy) layers contain massive elements of C, Mo, and S, compared to those in region marked by F. Hence, it can be concluded that a great deal of MWCNTs are pulled out from TMC-MM, worn out, repaved, and made to adhere onto wear scar at 0.7 m/s-16.3 N.

Figure 12 shows the higher magnification image performed in the region marked by rectangle in Fig. 10(b). As can be seen from Fig. 12, C element is found to gather abundantly close to smooth isolated island-like (patchy) layers, and made to tightly adhere onto wear scar by MoS_2 (see Fig. 12e, f).

Based on the detailed results of Table 2, and Fig. 10(d) and 12, it can be concluded that massive MWCNTs are first pulled out from TMC-MM at 0.7 m/s-16.3 N, and made to tightly adhere on to wear scar by MoS_2. Second, MWCNTs are uniformly spread out on wear scar, and accumulated into the smooth isolated island-like (patchy) layers due to the effect of sliding frictional force. Third, the repaved MWCNTs serve as the spacers between GCr15 ball and TMC-MM during the dry sliding wear, resulting in the formation of the smooth isolated island-like (patchy) layers. Eventually, they carry the load of GCr15 ball, and protect TMC-MM from being further destroyed, thereby increasing the SHWS and acquiring an
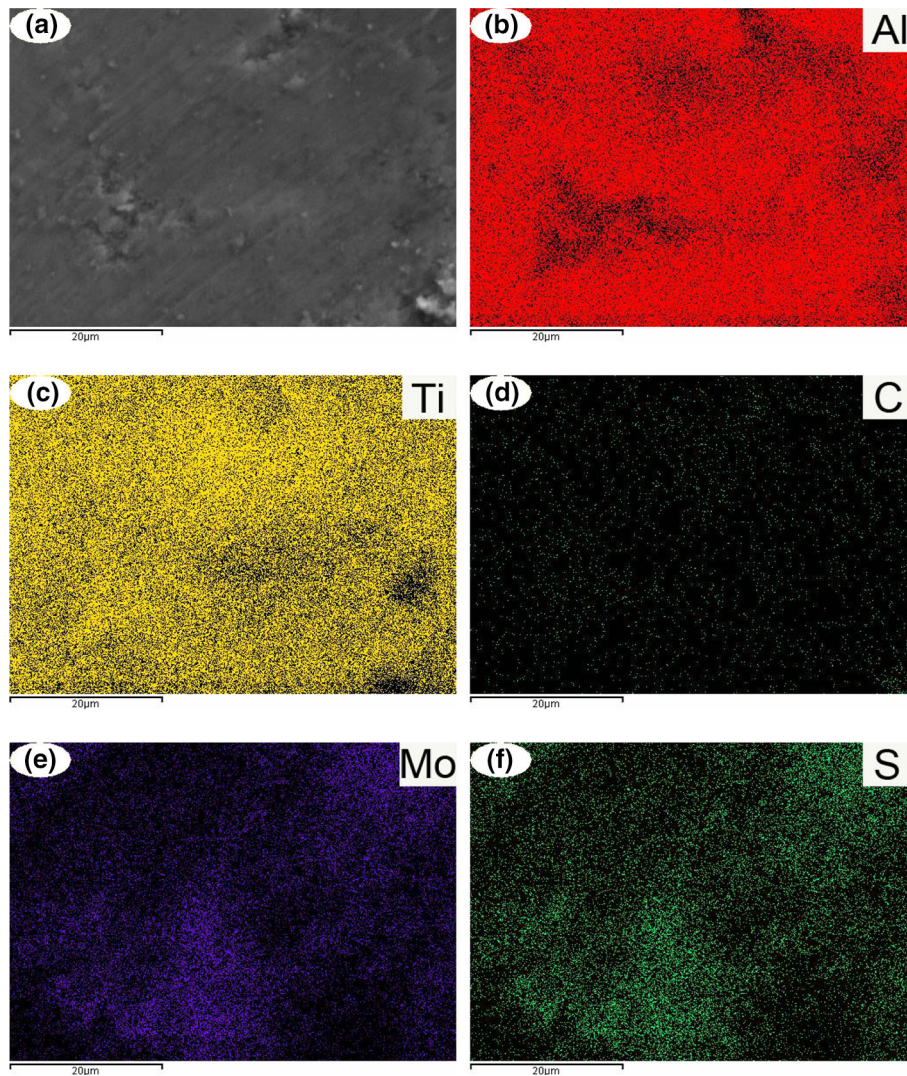
Fig. 11 Microstructural and elemental distributions of local wear scar marked by rectangle in Fig. 10(a)

Table 2 Elemental compositions (at.%) of measured regions marked by D, E, and F in Fig. 10(b)

Element	C	Mo	S	O	Fe	Ti	Al	Cr	Nb	Si
D	…	1.78	1.83	14.81	2.12	37.01	36.32	1.35	1.66	1.03
E	23.91	1.89	1.79	13.37	0.63	25.52	31.27	1.6	…	…	…
F	12.41	3.14	3.09	8.58	2.46	31.23	32.31	…	3.87	2.85

excellent tribological behavior at 0.7 m/s-16.3 N. Hence, it could be concluded that the excellent tribological behavior of TMC-MM at 0.7 m/s-16.3 N is closely related with the smooth isolated island-like (patchy) layers.

3.6 Surface Texture of Wear Scar

The surface texture of wear scar can be evaluated by the height parameters, such as Sa (arithmetical mean height), Sq (root mean square height), Sku (height distribution kurtosis), and Ssk (height distribution skewness).

Figure 13 shows the typical surface textures of wear scars at 0.3 m/s-6.5 N and at 0.7 m/s-16.3 N. As shown in Fig. 13(b), the small height parameters (Sa:0.66, Sq:0.56, Sku:8.21, and

Ssk:−0.16) of surface textures of wear scars are obtained because of the formation of the smooth isolated island-like (patchy) layers at 0.7 m/s-16.3 N, compared to those at 0.3 m/s-6.5 N (see Fig. 13a).

In order to better explore the tribological behavior of TMC-MM, the wear scar cross sections of TMC-MM need to be further studied at 0.3 m/s-6.5 N and at 0.7 m/s-16.3 N respectively.

3.7 Cross-Sectional Analysis of Wear Scar of TMC-MM

Figure 14 exhibits the typical FESEM micrographs of wear scar cross sections obtained after 80-min sliding at 0.3 m/s-6.5 N and 0.7 m/s-16.3 N. The positions of wear scar cross
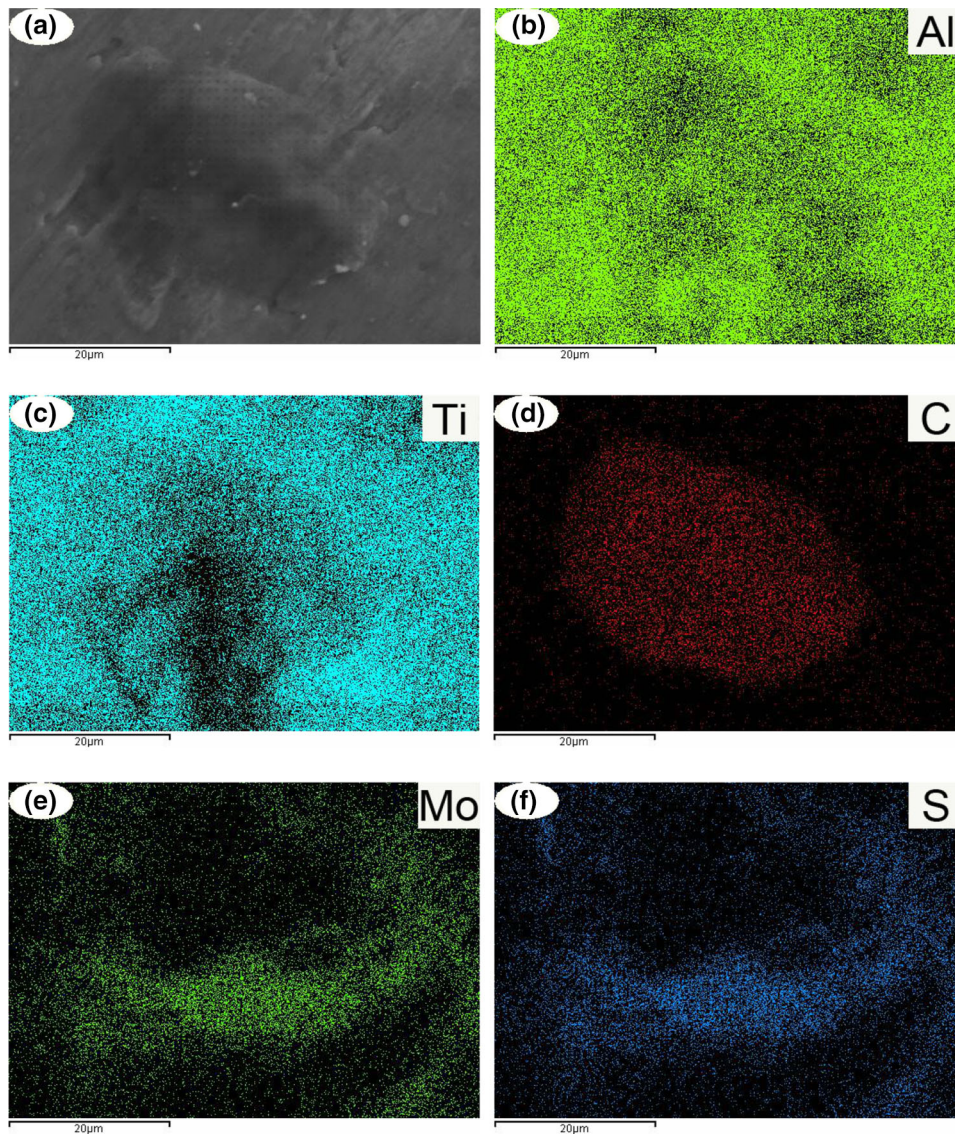
Fig. 12 Higher magnification image and elemental distributions performed in the region marked by rectangle in Fig. 10(b)

sections are marked by straight lines, as shown in Fig. 10(a) and (b). The significant stratification morphologies are clearly identified in Fig. 14. As shown in Fig. 14(a), the two stratified morphologies are observed at 0.3 m/s-6.5 N. Layer A is known as the compacted layer for the existence of submicron grains. Layer B is named as the substrate material of TMC-MM. As shown in Fig. 14(b), layer C, layer D and layer E are formed at 0.7 m/s-16.3 N. Layer C, layer D and layer E are known as the lubrication film, the compacted layer and the substrate material of TMC-MM, respectively. Hence, the small friction coefficient and wear rate are obtained for the forming of lubrication film at 0.7 m/s-16.3 N.

3.8 Mechanism Analysis of TMC-MM

Figure 15 shows the schematic diagrams of cross-sectional microstructures of wear scars of TMC-MM at 0.3 m/s-6.5 N and 0.7 m/s-16.3 N. As shown in Fig. 15(a), the stratified morphologies of the compacted layer and the substrate material

of TMC-MM are clearly exhibited. However, the lubrication film is not formed at 0.3 m/s-6.5 N. It leaded to the poor tribological behavior. As shown in Fig. 15(b), the stratification morphologies of the lubrication film, compacted layer and substrate material of TMC-MM are clearly observed at 0.7 m/s-16.3 N. Firstly, massive MWCNTs pulled out from TMC-MM during the dry sliding process are accumulated into the smooth isolated island-like (patchy) layers for the effect of sliding friction force. Secondly, MoS_2 with high adhesive behavior is continually enriched to wear scar during the sliding wear. Eventually, massive MWCNTs on wear scar are tightly adhered to wear scar by massive MoS_2 at 0.7 m/s-16.3 N, and uniformly spread out to form lubrication film. The smooth isolated island-like (patchy) layers containing massive MWCNTs could serve as the spacers, and carry the load of GCr15 ball during the 80-min sliding wear. It is beneficial to the formation of lubricating film and the protection of TMC-MM from further damage, resulting in the lower friction coefficient and less wear rate at 0.7 m/s-16.3 N.
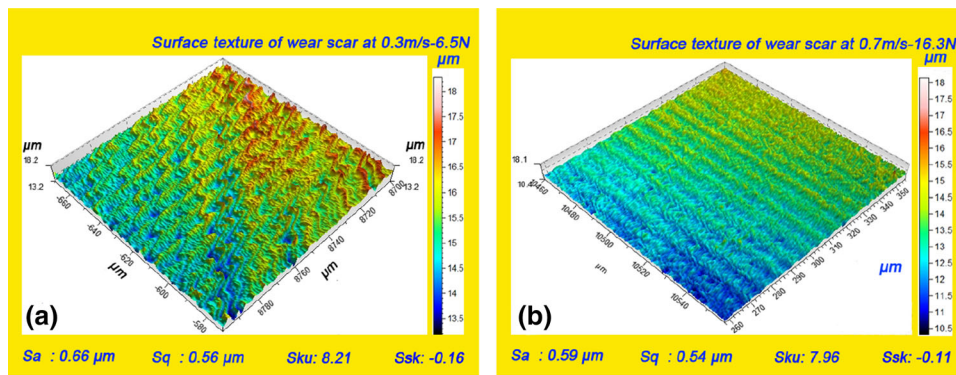
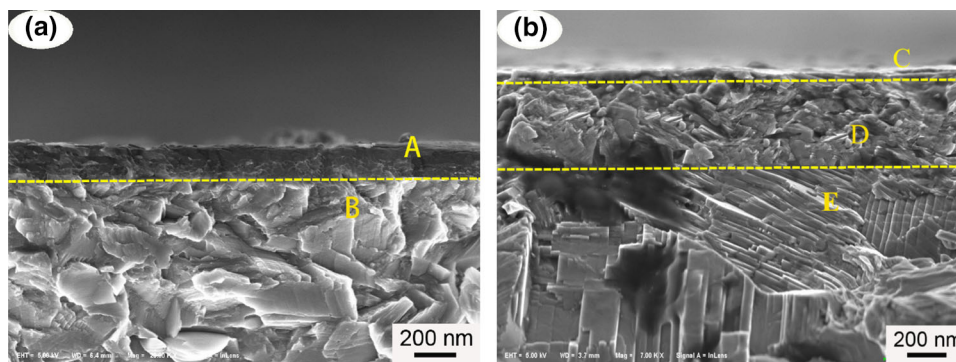**Fig. 13** Typical surface textures of wear scars at 0.3 m/s-6.5 N (a) and at 0.7 m/s-16.3 N (b)

Fig. 14 Typical FESEM micrographs of wear scar cross sections obtained after 80-min sliding at 0.3 m/s-6.5 N (a) and 0.7 m/s-16.3 N (b)
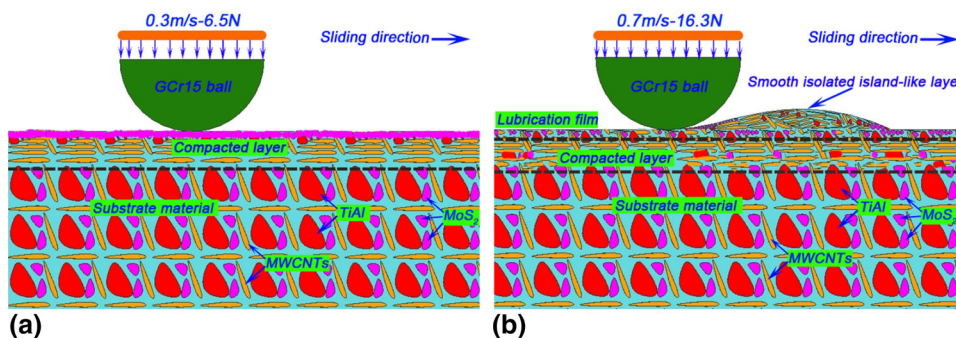

Fig. 15 Schematic diagrams of cross-sectional microstructures of wear scars of TMC-MM at 0.3 m/s-6.5 N (a) and at 0.7 m/s-16.3 N (b)

4. Conclusions

In this study, the tribological behaviors of TiAl substrate composite containing MWCNTs and MoS_2 (TMC-MM) are investigated at 0.3 m/s-6.5 N, 0.5 m/s-11.4 N, and 0.7 m/s-16.3 N, respectively. Three conclusions are obtained as follows:

1. The excellent tribological behavior of TMC-MM is obtained because of the formation of lubricating film containing massive MWCNTs and MoS_2 at 0.7 m/s-16.3 N.
2. The formed smooth isolated island-like (patchy) layers could effectively protect lubricating film from being further destroyed at 0.7 m/s-16.3 N.

3. The high SHWS (8.2 GPa) at 0.7 m/s-16.3 N is attributed to the formation of the smooth isolated island-like (patchy) layers containing massive MWCNTs of high hardness on the worn surface of TMC-MM.

References

1. S.Y. Sung and Y.J. Kim, Modeling of Titanium Aluminides Turbo-Charger Casting, *Intermetallics*, 2007, **15**, p 468–474
2. X.H. Wu, Review of Alloy and Process Development of TiAl Alloys, *Intermetallics*, 2006, **14**, p 1114–1122
3. C.M. Austin, Current Status of Gamma Ti Aluminides for Aerospace Applications, *Curr. Opin. Solid State Mater. Sci.*, 1999, **4**, p 239–242
4. C.Q. Peng, B.Y. Huang, and Y.H. He, Effects of Alloying on Properties of TiAl-Based Alloys and Mechanisms, *T. Nonferr. Metal. Soc.*, 1998, **8**, p 11–16
5. J. Cheng, Y. Yu, L.C. Fu, F. Li, Z.H. Qiao, and J.S. Li, Effect of TiB_2 on Dry-Sliding Tribological Properties of TiAl Intermetallics, *Tribol. Int.*, 2013, **62**, p 91–99
6. T. Sun, Q.D. Wang, L. Sun, G.H. Wu, and Y. Na, Study on Dry Sliding Friction and Wear Properties of Ti_2AlN/TiAl Composite, *Wear*, 2010, **268**, p 693–699
7. X.L. Shi, Z.S. Xu, M. Wang, W.Z. Zhai, J. Yao, and S.Y. Song, Tribological Behavior of TiAl Matrix Self-Lubricating Composites Containing Silver from 25 to 800 °C, *Wear*, 2013, **303**(1-2), p 486–494
8. J.L. Li, D.S. Xiong, and Y. Wan, Effect of Counterface Material on Friction and Wear Behavior of Ni-Cr-W-Al-Ti- MoS_2 Composite, *Chinese J. Aero.*, 2006, **19**, p 74–79
9. S. Mahathanabodee, T. Palathai, S. Raadnui, R. Tongsri, and N. Sombatsompop, Dry Sliding wear Behavior of SS316L Composites Containing h-BN And MoS_2 Solid Lubricants, *Wear*, 2014, **316**, p 37–48
10. I. Ahmad, A. Kennedy, and Y.Q. Zhu, Wear-Resistant Properties of Multiwalled Carbon Nanotube-Reinforced Al_2O_3 Nanocomposites, *Wear*, 2010, **269**, p 71–78
11. M. Mina, H. Bastwros, M.K. Amal, and E.A. Wifi, Friction and Wear Behavior of Al-CNT Composites, *Wear*, 2013, **307**, p 164–173
12. American Society for Testing and Materials, Standard test method for vicker's hardness of metallic materials, ASTM E92-82 e2, 2003
13. American Society for Testing and Materials, Standard test methods for density of compacted or sintered powder metallurgy (PM) products using Archimedes' principle, ASTM B962-08, 2008
14. American Society for Testing and Materials, Standard test method for wear testing with a pin-on-disk apparatus, ASTM G99-95, 1995
15. S.S. Fang, M.Y. Sun, Y.W. Zhou, Q. Liang, Z.Y. Li, and S. Xu, Solvothermal Synthesis of CdS QDs/MWCNTs Nanocomposites with high Efficient Photocatalytic Activity Under Visible Light Irradiation, *J. Alloy Compd.*, 2016, **656**, p 771–776
16. D.W. Ma, W.W. Ju, T.X. Li, X.W. Zhang, C.Z. He, B.Y. Mab, Y.A. Tang, Z.S. Lu, and Z.X. Yang, Modulating Electronic, Magnetic and Chemical Properties of MoS_2 Monolayer Sheets by Substitutional Doping with Transition Metals, *Appl. Surf. Sci.*, 2016, **364**, p 181–189
17. R.D. Tyagi, S. Xiong, and J.L. Li, Effect of Load and Sliding Speed on Friction and Wear Behavior of Silver/h-BN Containing Ni-Base P/M Composites, *Wear*, 2011, **270**, p 423–430
18. I. Ahmad, A. Kennedy, and Y.Q. Zhu, Wear Resistant Properties of Multi-walled Carbon Nanotubes Reinforced Al_2O_3 Nanocomposites, *Wear*, 2010, **269**, p 71–78